BioChip J. (2013) 7(2): 95-103
DOI 10.1007/s13206-013-7203-y

Original Article

High-speed three-dimensional characterization of fluid flows induced by micro-objects in deep microchannels

Chia-Yuan Chen[1] **& Kerem Pekkan**[2,3]

Received: 7 February 2013 / Accepted: 1 April 2013 / Published online: 20 June 2013

Abstract Bio-inspired studies of micro-objects in microfluidics demand quantitative microflow visualization tools to evaluate their three-dimensional (3D) fluid dynamic performance. Experimental fluid dynamic measurements of bio-hybrid systems are employed when non-traditional small-scales, magnetohydrodynamic coupling and nonlinear material properties are involved. In this study a stereoscopic micro-Particle Image Velocimetry (μPIV) system was developed to characterize instantaneous flow fields induced by (1) a micro-robot ($280 \times 200 \times 150\ \mu m^3$) and (2) self-assembled magnetically actuated artificial cilia (~50 μm in diameter and 500 μm in depth). A custom built micro jet flow microchannel was tested to provide the quantitative evidence of measurement accuracy with 14% error compared to theoretical solutions in the out-of-plane velocity component. Followed by these verification experiments, instantaneous in-plane spinning motion was analyzed in conjunction with translational movement and out-of-plane rotational movements of the micro-robot to obtain the induced 2D-3C (two-dimension, three-component) fluid velocity data. The second test case investigated the micro-scale vortical flow structures that were generated by self-assembled magnetically driven artificial cilia. The strength of this 3D micro vortex structure was computed based on the 3D flow measurements. In combination with the asymmetric cyclic motion of the magnetically actuated artificial cilia, it is expected that these structures can generate transverse flow efficiently in 3D, and thus provide a potential alternative for mixing in low Reynolds number flows, analogous to a micromixer. The acquired 3D microflow field, along with the validation tests, further extends the capability of using stereoscopic μPIV technique to evaluate the performance of noninvasive microflow manipulators.

Keywords: Micro particle image velocimetry, PIV, micro-robot, Artificial cilia, Biomimetics

Introduction

Micro-Particle Image Velocimetry (μPIV) is an established experimental technique for evaluating the performance of microfluidic and biomedical devices[1] and for understanding the swimming behavior of microorganisms (e.g. Paramecia, plankton species)[2]. This measurement technique provides high spatial resolution ($\sim 10^{-1}$ μm) and typically two velocity components[3]. Associated with its typically tedious calibration process in three-dimensional (3D) flows the majority of μPIV studies to date were conducted in two-dimensional (2D) microflow configurations. However, microfluidic devices that can induce three-component (3C) velocity fields, such as micromixers and micropumps, provide improved performance than those that can only generate two-component (2C) velocity fields. Thus, there has been an increasing trend to develop a 3C velocity measurement technique for 3D microflow visualization in recent years[4]. Additionally, 3D hydrodynamic focusing has become an effective high-throughput flow cytometry technique[5] because of its ability

[1]Department of Mechanical Engineering, National Taiwan University of Science and Technology, Taipei 10607, Taiwan
[2]Department of Biomedical and Mechanical Engineering, Carnegie Mellon University, Pittsburgh, PA 15219, USA
[3]Department of Mechanical Engineering, Koc University, Rumelifeneri, Istanbul, Turkey
Correspondence and requests for materials should be addressed to K. Pekkan (✉kpekkan@andrew.cmu.edu)

to accurately control focal position. Still 3D precise control of sheet flows requires real-time 3D flow visualization data. For example, accurate evaluation of artificial cilia that function as micropumps or micromixers in microfluidics has been addressed previously with 2D μPIV flow measurement[6]. Acquired 3D μPIV flow data can be calculated for volume flow rates along the out-of-plane direction, thus allowing greater control of micromixing and improved performance. Furthermore, 3D microcavities having sharp corners can trigger complex flow separation due to their channel geometry. Calculation of flow parameters such as vorticity and circulation[7] using 3D μPIV data can further optimize the performance of existing designs. Therefore, a μPIV system with 3D flow data acquisition capability is an essential element for effective microfluidic devices.

In this study, a custom designed high-speed stereoscopic μPIV system was assembled to quantify induced flow structures by (1) a micro-robot and (2) self-assembled magnetically actuated artificial cilia. The instantaneous 2D-3C velocity data demonstrate the capability of evaluating (1) a micro-robot's operating performance at low Reynolds number regime for future remote control improvement; and (2) a potential application of self-assembled magnetic artificial chain-like structures to generate a 3D vortex, for operation as an efficient micromixer.

Advances of the "Lab on a chip" concept improve traditional time-consuming and high cost of bio-sample analysis techniques in the lab[8]. A key aspect of lab chips concerns rapid and complete mixing of test samples with chemical solute streams[9] at low cost[8]. However, fast and efficient mixing is still challenging due to the sole micro scale mixing mechanism of low efficiency molecular diffusion across the species interfaces[10]. To increase the mixing efficiency, generation of transverse flows, in addition to the axial main flow, is a promising alternative. Two main strategies for generating transverse flow are (1) active mixing using external forces, such as magnetic force[11,12], electrostatic force[13] and light-driven force[14]; and (2) passive mixing using geometry designs such as staggered herringbone structures[15], serpentine channels[16] and planner spiral microchannels[17]. However, these techniques are not fully suitable for portable operation due to the designed lab chips require sophisticated multi-fabrication processes, weighty and complex control systems, and experienced operators. A potential alternative design for portable micromixer is self-assembled magnetically actuated artificial cilia.

Self-assembled magnetically actuated artificial cilia can be formed by simply applying an external magnetic field to the magnetically polarizable particles (NdFeB). A handful size of neodymium permanent magnets (~2.5 cm in diameter and 7.5 cm in depth) is enough to actuate these magnetic chains inside a deep PDMS (Polydimethylsiloxane) microchannel. These magnetized particles acquire dipole moments, and the induced moments interacting with each other lead to the formation of chain-like of particles aligned with the magnetic field direction[18]. Fabricated artificial cilia have several advantages over the previously mentioned techniques to active manipulation of flow fields in microscale. For example, these artificial cilia can be rotated through all axes without the loss of structural form[19], thus allow the generation of transverse flows for augmented mixing. Likewise, the formation of artificial cilia is reversible, allowing them to be formed and reformed spontaneously, depending on the presence of the magnetic field[19]. This feature that resembles polarization/depolarization is very suitable for portable use since there is no need for activation chemicals or complex control systems for artificial cilia deployment and operation. These characteristics make self-assembled artificial cilia as an ideal effective micromixer and flow-controller.

Microflow propulsion and control at low Reynolds numbers is governed through the well-known "Scallop Theorem"[20]. This theorem implies that for an efficient mixing the generation of nonreciprocal motion through the artificial cilia is required. In this study, nonreciprocal motions of chain structures were actuated practically using two external magnets with a separation angle of 90°. Complex flow tasks such as the generation 3D microflow vortex and an asymmetric dipole vortex were generated by the asymmetric dynamic motion of artificial cilia. Existence of these complex flow structures were confirmed using the stereoscopic μPIV measurements described in the Results section.

Results and Discussion

Validation test for the accuracy of the out-of-plane velocity calculation

A low Reynolds number ($Re < 1$) micro jet flow is generated inside a test micro channel to validate the accuracy of out-of-plane velocity acquisition from our stereoscopic μPIV algorithm protocol. In Figure 1A, the inflow direction of this micro jet is indicated by an arrow inside our test microchannel. The stereoscopic μPIV system was arranged so that time-resolved stereo image pairs were recorded from the thin cover slip. The effective region of interest (570×400 μm^2) of the micro jet flow inlet measurement plane, which is located at the bottom wall of the micro-

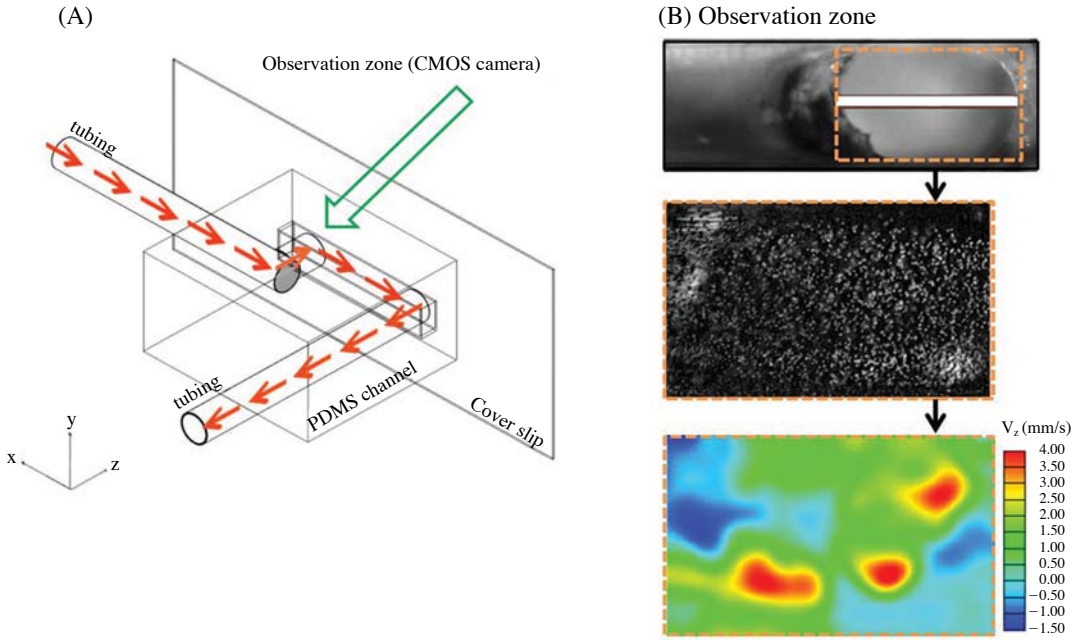

Figure 1. (A) Schematic illustration of the micro jet flow validation test chamber. Region of Interest is indicated with a green arrow. (B) From top to bottom: a circular opening having an effective rectangular area of $570 \times 400\ \mu m^2$ was drilled at the bottom wall of the microchannel (top); corresponding μPIV particle raw image (middle); corresponding stereoscopic μPIV calculated out-of-plane (V_z) results (bottom). The dashed orange rectangle indicates the effective region of interest with unchanged $570 \times 400\ \mu m^2$ size. White color bar: 570 μm.

channel, as well as stereo-calibrated μPIV images are presented in Figure 1B. The corresponding μPIV out-of-plane velocity data (V_z) in this region of interest is also shown as a contour plot (See Figure 1B). The non-uniform flow distribution was caused by a developing velocity profile resulted from the curved inlet upstream section. In order to estimate the accuracy of our stereoscopic μPIV protocol, the presented data were compared to theoretical values. The theoretical average velocity value of the jet flow that emerged out of the opening of our micro-channel bottom (based on its physical dimensions $570 \times 400\ \mu m^2$) was calculated as 1.46 mm/s considering a steady flow rate of 20 μL/min. After flowing out the opening, this jet flow branched into two flow streams due to the geometry of the microchannel. One stream flowed along z-direction and the other flowed along negative x-direction. It is suggested that the out-of-plane (along z-direction) velocity was inversely proportional to the distance from the bottom wall of the microchannel due to the pressure drop was along the negative x-direction. The decrease of the out-of-plane velocity was compensated by the increase of the in-plane velocity along the negative x-direction to satisfy the mass conservation equation, as our results indicated. As the position of the stereoscopic PIV measurement plane in this test was 350 μm above the bottom wall of the microchannel, Therefore the entrance jet flow velocity,1.46 mm/s, was decreased with a ratio of 1/2 (350 μm/700 μm, 700 μm is the depth of the microchannel) leading to a theoretical value of 0.73 mm/s on our stereoscopic μPIV measurement plane[21]. Likewise, the corresponding average velocity obtained through stereoscopic μPIV measurements is 0.85 mm/s. The out-of-plane error was therefore calculated to be 14%, which is acceptable for microflow quantification in 3D measurements. Note that this calculation is based on circular idealized unbounded jets; non-uniform jet cross-section and channel walls as employed in our channel would influence this theoretical estimate. This error serves as a baseline for future improvements to this technique

Test case 1: Internal flow fields induced by a single micro-robot

A rectangular magnetic micro-robot ($280 \times 200 \times 150\ \mu m^3$) was operated in a deep microchannel as shown in Figure 2A. A rotating applied field of 20 mT with a permanent magnet is used for actuation and control. The instantaneous PIV velocity vectors of the in-plane rotational and translational motions induced by the micro-robot inside a microchannel are shown in Figure 2B. Instantaneous contour velocity maps provide fur-

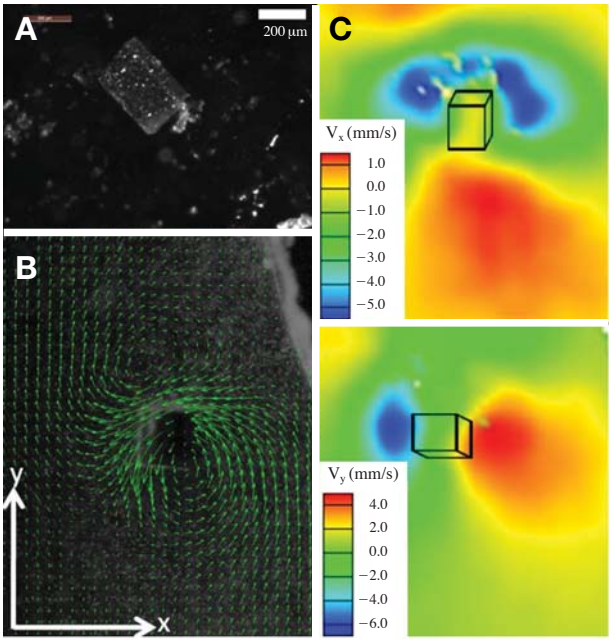

Figure 2. (A) Image of the stationary magnetic micro-robot before magnetic field application. (B) Overlay image of tracing particles and a sample instantaneous μPIV velocity vector field (green) during in-plane rotational and trans-lational motions of the micro-robot. (C) Velocity contour plots for x- (top) and y- (bottom) velocity components. An outline of the micro-robot is sketched on contour plots.

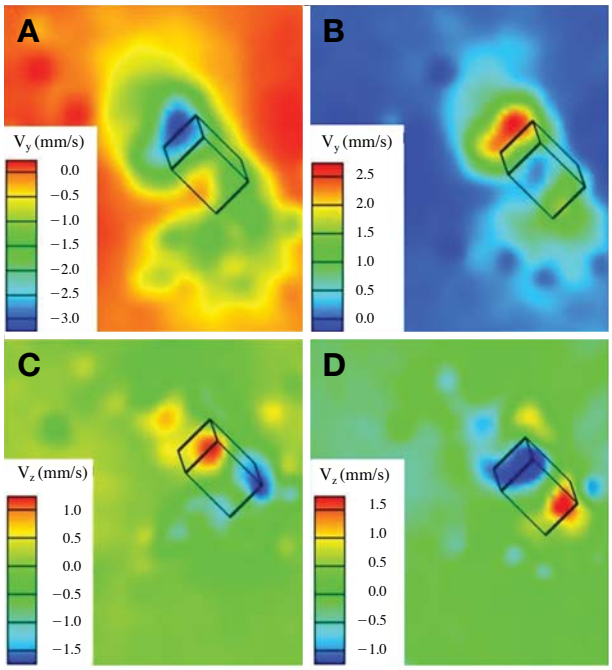

Figure 3. PIV time-series sum of correlation velocity distribution contour plots during micro-robot out-of-plane rotation. Velocity distribution in y direction during counter-clockwise (A) and clockwise (B) rotational phases. Corresponding out-of-plane velocity distribution of counter-clockwise (C) and clockwise (D) rotational phases. An outline of the micro-robot is sketched on contour plots.

ther quantitative information during these fundamental motions (Figure 2C). As expected, due to the movement of an external magnet driven, the in-plane velocity component V_x is slightly higher in the upper regions of the microchannel, resulting in a leftward movement of the micro-robot at 4 mm/s. Additionally, the central region of the V_y contour plot shows negative velocity on the left side and positive on the right, demonstrating counter-clockwise rotation (up to 5 mm/s) of the fluid.

In addition to the in-plane translation test, an out-of-plane rotation along the transverse axis was also specified on the micro-robot. For this movement negative velocity values appeared in the central region of the V_y component contour plot (Figure 3A). Likewise for the V_z component contour plot, positive values appeared in the upper central region and negative values in the lower central region (Figure 3C). These flow measurements agreed the physical movement of the micro-robot, where out-of-plane counter-clockwise rotation near the bottom wall accompanied an in-plane receding movement. Velocity contour plots of the same movement type but with clockwise micro-robot rotation are shown in Figure 3B and 3D. As expected, out-of-plane clockwise rotation showed positive values in the lower and negative values in the upper regions of the V_z component contour plot (Figure 3D), as well as positive values of the V_y component (Figure 3B). These flow structures can be further utilized to flip larger objects, such as the embryo in a confined microchannel, for different anatomical views during imaging or can be repeated in complex fluids.

Test case 2: Flow patterns induced by the magnetically actuated artificial cilia

Two types of vortices were generated using self-assembled artificial cilia and acquired using stereoscopic μPIV. The first major vortex pattern is an asymmetric 3D vortex flow structure as shown in Figure 4A & B. The streamtraces are shown as contour plots displaying the area of the induced vortex core along z-, x- and y- directions in Figure 4C, 4D and 4E, respectively. In Figure 4C (in out-of-plane direction), negative values appeared on the left while positive values appeared on the right, showing out-of-plane counter-clockwise rotation along *x*-axis. In terms of in-plane induced flow structure, as shown in Figure 4D and E in x and y directions, respectively, a vortex with clockwise

rotation was found and visualized using 2D streamtraces, outlined in black lines. The magnitude of peak velocity in the out-of-plane direction reaches 1.5 mm/s, which is higher than in-plane peak velocity components (1 mm/s). This implies that these artificial cilia are able to induce micro flow in 3D. Potentially, global 3D mixing inside a microchannel may be achieved if a series of these artificial cilia can be synchronized and actuated to generate this type of vortex. The second type of vortex generated by artificial cilia was a dipole vortex with asymmetric vortex structure, which was analyzed through the stereoscopic μPIV measurements. Two vortex rings with opposite signs of circulation and magnitudes, outlined with 2D streamtraces, are presented in the Figure 5. A clockwise vortex ring with relative large circulation appeared in the upper region, while the vortex ring with counterclockwise rotation direction appeared in the bottom region of the channel. When the artificial cilia were actuated in the opposite direction (toward to the right), similar vortex structures but with the opposite circulations were generated, (Figure 5, right panel). The implications of these vortices, and other observed phenomena, were explored further through quantitative analysis in the Discussion section.

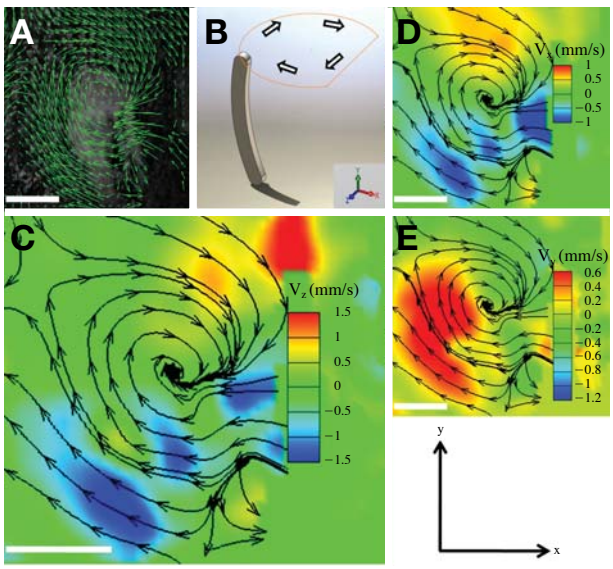

Figure 4. Stereoscopic μPIV analysis of an asymmetric 3D vortex induced by a self-assembled magnetically artificial cilium in a microchannel. (A) Overlay image of tracing particles and instantaneous μPIV velocity vectors (green). (B) Cartoon illustration of artificial cilium's cyclic motion. (C-E) Velocity contour plots for z- (C), x- (D), and y-(E) velocity components. 2D streamtraces are plotted on contour plots to indicate vortex flow structure. White scalar bar: 100 μm.

There are a number of μPIV techniques having the capability to acquire velocity components along the three directions, such as holographic PIV[22], tomographic PIV[23], confocal μPIV[24], and the stereoscopic μPIV with rotational optical set-up as proposed in this work. Main weaknesses of holographic PIV is the requirement of recording large number of holograms in order to reach a stable statistics[25]. A tomographic PIV technique requires more than two cameras (usually four) to acquire several simultaneous views of particles in a flow domain. Sophisticated volumetric image reconstruction is necessary to obtain 3D velocity from cubic interrogation windows. Due to the requirement of multiple camera synchronization, the accompanied vibration, cost and high heat dissipation pose major problems. Nevertheless, the tomographic acquisition is a "real" 3D PIV method since the cubic voxel data at any measurement domain is acquired. In the stereoscopic

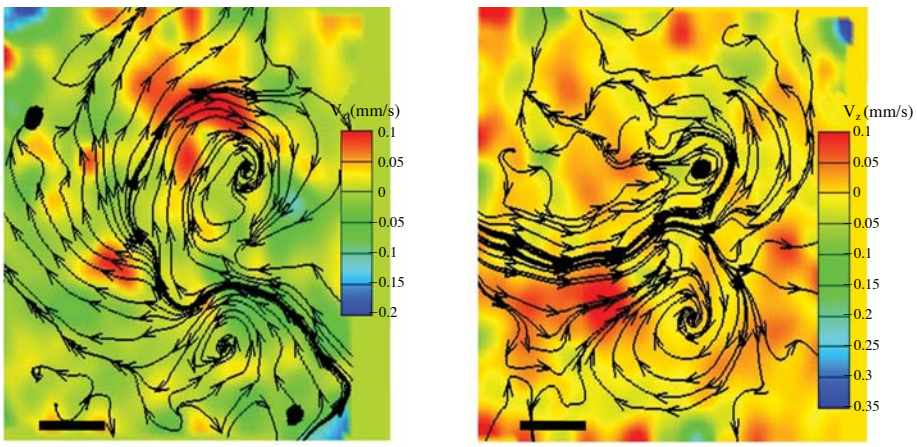

Figure 5. Stereoscopic μPIV analysis of two asymmetric dipole vortices with opposite main flow directions induced by a self-assembled magnetically actuated artificial cilium in a microchannel. Flow direction toward left (left panel) or to the right (right panel). Black scalar bar: 100 μm.

μPIV technique the 3D data can be calculated only on the measured sheet plane. Confocal μPIV is also a promising method with better resolution (10^0 μm) than the stereoscopic method (10^1 μm)[26]. Still, high complexity and low scanning speed of optical set-up hampers the practical use Confocal μPIV as a 3D measurement tool.

For microscopic flow control, the fast acquisition of the instantaneous induced flow structures, as well as the image data quality is critical for accurate PIV results. The recording frame rates performed in this study ranged from 30 to 125 Hz. Higher frames rates are possible for the camera used (up to 3600 Hz) with decayed particle intensity; however, faster recording rate also means low exposure time. Decreased signal-to-noise ratio has a negative effect on PIV calculation and additional image pre-processing methods may be required. The flow tracer contrast relative to background noise is further improved by a number of image pre-processing methods[27]. Basic image processing operations such as the subtraction of sliding minimum intensity over time, are executed before stereosopic μPIV calculation. Likewise, averaging a set of time-series images can reveal the background noise pattern. By subtracting the noise from each raw image, a new series of processed images can be obtained. Moreover, a pre-processing method called "Subtract sliding background" acts as a high pass filter for large intensity fluctuations in the background. These standard methods are handy in dealing with non-uniform flow fields.

In Test Case 1, the micro-robot was able to induce an in-plane vortex as well as out-of-plane flow patterns. However, as illustrated in Figure 2B-D, the micro-robot can only influence a finite surrounding flow region inside the microchannel, where the viscous force is dominant. The volume of the induced flow field is equivalent to around six micro-robot volumes. This matches a previous study that used dimensionless analysis to demonstrate that local microscale stirring is very inefficient for mixing applications in large chambers[20]. However, the use of large number of mixing robots can further improve mixing and transport. Using large number of magnetic particles can be a good alternative to using glass capillaries for manipulation of microorganisms for time-lapse imaging.

As a first step toward understanding cilia motions, biomimetic studies using self-assembled magnetically actuated artificial cilia were conducted and in the current study, analyzed in Test Case 2. Previous studies focusing on self-assembled magnetically actuated artificial cilia mainly used numerical methods[18,28] and detailed 3D experimental flow field quantification data are absent[19]. One recent study was done with μPIV using two cameras to quantify induced flow field by artificial cilia[6], which are similar to our artificial cilia, in a microchannel. However, only in-plane velocity data across entire flow domain were acquired and presented. In the present study, 2D-3C surrounding flow velocity data induced by magnetically actuated artificial cilia were measured and quantified. The unique contribution of stereoscopic μPIV compared to conventional 2D μPIV is its ability to quantify velocity in the out-of-plane direction. This characteristic is vital to Test Case 2 as shown in Figure 4, where the generated 3D vortex has the largest velocity magnitude along out-of-plane axis, in contrast to in-plane. The induced flow magnitude and cilia performance can be underestimated through the 2D μPIV data. Moreover, artificial cilia exhibit asymmetrical cyclic motion (Figure 4), where positive velocity values spread over the region, while negative values only appeared in a small region. This type of asymmetric motion is essential to generate flow propulsion in low Reynolds number for potential microflow manipulation applications such as micromixers and micropumps.

Two types of vortices were investigated in Test Case 2. To compare their magnitude the amount of flow that circulates in each vortex ring was quantified (Figure 6). Specifically, three equal size circular zones (radius=100 μm) were created. Velocity vectors dotted with unit tangential were integrated through the edge of each circular zone. Results show that the circulation of the 3D vortex is $-0.335\ mm^2/s$, and the two symmetric dipole vortex rings are $-0.019\ mm^2/s$ and $0.005\ mm^2/s$ respectively. Computed circulation values match the micro-robot movement where a negative sign represents clockwise rotation and vice versa. The difference in magnitude of the dipole vortices was due to the uneven influence of the magnet, which was oriented on the right side of the artificial cilia. It suggests that the asymmetry of the vortices can be manipulated by the positioning of the rotating magnet. More complex flow patterns can be generated by additional magnets. The circulation level is also adjustable by changing the magnitude of the magnetic field. Most importantly, the reported data demonstrate the capability of using stereoscopic μPIV technique to evaluate the performance of microfluidic devices and provide a way for acquiring information that is vital for feedback control of such devices.

Conclusions

A stereoscopic μPIV technique was reported to quan-

titatively describe 3D flow fields induced by micro-objects, including a micro-robot and self-assembled magnetically actuated artificial cilia. The reported first test case has potential applications in new designs of micro-organism monitoring tools and the second text case can be used to generate transverse flow for micro scale mixing applications. These induced flow field data analyzed by stereoscopic μPIV can be presented as feedback information for a remote control system for real-time adjustment of its magnetic field magnitude accordingly on each application. Additionally, with proper image pre-processing methods, stereoscopic μPIV calculation of periodic micro-object motions becomes achievable. The results of the reported test cases demonstrate the diversity of microfluidic applications using stereoscopic μPIV.

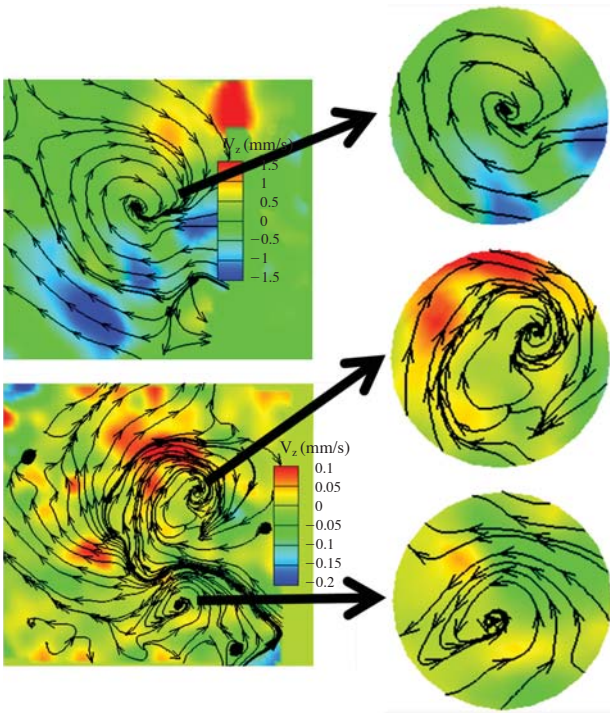

Figure 6. Circulation analysis of generated vortices by self-assembled artificial cilia. Circles from top: (1) vortex ring of a 3D vortex (circulation = −0.335 mm^2/s); (2) upper vortex ring of an asymmetric dipole vortex (circulation = −0.019 mm^2/s); (3) bottom vortex ring (circulation = +0.005 mm^2/s). Circle radius: 100 μm. Negative sign represent clockwise circulation, and vice versa.

Materials and Methods

Microchannel fabrication and artificial cilia actuation

Deep polydimethylsiloxane (PDMS) microchannels were fabricated first using a standard photolithography process to make an SU-8 mold[24], followed by PDMS casting and finally bound to a cover slip through oxygen plasma bombardment. Two-time spin coating of SU-8 photoresist on the silicon wafer was applied, resulting an SU-8 mold over 500 μm in thickness. The manufacturing and operation of the micro-robot system is described in earlier publications[29] by embedding NdFeB particles into a polyurethane binding agent and molded to the desired shape. The actuation of the artificial cilia was through a rotary motor (Pololu Corp., NV) with a permanent magnet (K&J Magnetics Inc., PA) attached to it. A magnetic coil system is an alternative method to generate a homogenous magnetic field to specify more complex rotational motions to the artificial cilia.

Stereoscopic μPIV

The horizontal-layout stereoscopic μPIV system is

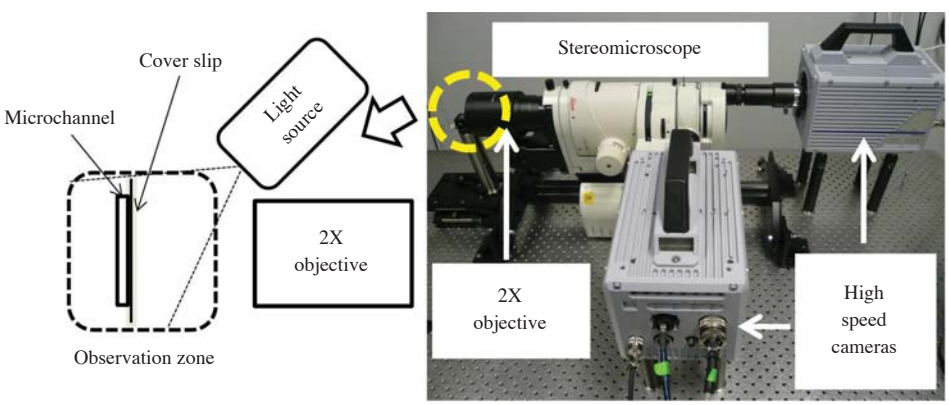

Figure 7. Configuration of the time-resolved stereoscopic μPIV system attached to the Leica MZ16FA stereomicroscope, in horizontal layout.

composed of a stereo-fluorescence microscope (Leica MZ16FA with Plan Apo 2X objective), two high speed cameras (Photron, USA), a Nd:YLF laser (Litron Lasers, England), a fibre optic light source illuminator (Fostec, Republic of Korea), a programmable timing trigger unit (LaVision, Inc., MI) for synchronization between the cameras and the laser, and a computer system for data acquisition. The configuration of the stereoscopic μPIV is shown in Figure 7. Fluorescent particles, 3.2 μm diameter (Microgenics, Inc., CA), were added to the microchannel so that the surrounding flow could be studied. Because a μPIV experiment is performed using volume illumination (as opposed to sheet illumination in standard PIV)[1], a laser-less continuous illumination by the optic light source illuminator and two high speed cameras were used for time-lapse raw particle image acquisition. The time between two consecutive particle images was determined by the camera frame rate (for present experiments, 125 Hz was sufficient).

A standard stereo calibration process was applied using a polygon-mapping function (LaVision, Inc., MI), employing a micro-calibration plate followed by the self-calibration process[30]. The root mean square (RMS) fitting error of the stereo calibration and the average deviation value of the self-calibration were <0.47 pixel and <0.1 pixel, respectively. All calibrated images were then processed using DaVis 7.2 PIV software using a stereoscopic velocity field calculation algorithm[31]. For uniform rotating micro-robot experiments (i.e. a complete counter-clockwise rotation or clockwise rotation cycle) phase-locked PIV analysis with sum of correlation algorithm was employed. The first-pass PIV interrogation window was 16×16-pixel with 50% overlap for 2 iterations, and the second-pass was 12×12-pixel interrogation size with 50% overlap for 2 iterations. Multi-pass post-processing median filtering was used to remove bad vectors >2 root mean square (RMS) and reinserted if <3 RMS of neighboring vectors.

Validation for stereoscopic μPIV using a micro jet flow microchannel

To test the accuracy of the velocity calculation in out-of-plane direction, a micro jet flow microchannel was first fabricated using the method described in the previous section. Specifically, at the observation zone, a hole was drilled from the cover slip side on the pre-fabricated PDMS microchannel bulk without punching through. Through the microscope measurement, this hole has an effective area of $570 \times 400\ \mu m^2$ at the bottom wall of the microchannel. Another hole with the same drill bit was then drilled from the other side of the PDMS microchannel bulk, and these two holes were intersected in the PDMS bulk. A schematic illustration of this micro jet flow microchannel is shown in Figure 1.

Acknowledgements The authors appreciate Metin Sitti, Eric Diller, and Zhou Ye for useful suggestions to micro-robot manipulation.

References

1. Lindken, R., Rossi, M., Grosse, S. & Westerweel, J. Micro-Particle Image Velocimetry (microPIV): recent developments, applications, and guidelines. *Lab on a chip* **9**, 2551-2567 (2009).
2. Chen, C.-Y., Chang, B.Y. & Pekkan, K. Feeding flow dynamics of developing zebrafish larvae. in 65th APS DFD Meeting (San Diego, California, USA, 2012).
3. Vennemann, P., Lindken, R. & Westerweel, J. In vivo whole-field blood velocity measurement techniques. *Experiments in Fluids* **42**, 495-511 (2007).
4. Erkan, N., Shinohara, K., Someya, S. & Okamoto, K. Three-component velocity measurement in microscale flows using time-resolved PIV. *Measurement Science & Technology* **19**, 057003 (2008).
5. Huang, T.J., Mao, X.L., Lin, S.C.S. & Dong, C. Single-layer planar on-chip flow cytometer using microfluidic drifting based three-dimensional (3D) hydrodynamic focusing. *Lab on a Chip* **9**, 1583-1589 (2009).
6. Hussong, J. *et al*. Experimental investigation of the flow induced by artificial cilia. *Lab on a Chip* **11**, 2017-2022 (2011).
7. Yu, Z.T.F., Lee, Y.K., Wong, M. & Zohar, Y. Fluid flows in microchannels with cavities. *Journal of Microelectromechanical Systems* **14**, 1386-1398 (2005).
8. Whitesides, G.M. What Comes Next? *Lab on a Chip* **11**, 191-193 (2011).
9. Khatavkar, V.V., Anderson, P.D., den Toonder, J.M.J. & Meijer, H.E.H. Active micromixer based on artificial cilia. *Physics of Fluids* **19**, 083605 (2007).
10. Kenis, P.J., Ismagilov, R.F. & Whitesides, G.M. Microfabrication inside capillaries using multiphase laminar flow patterning. *Science* **285**, 83-85 (1999).
11. Vilfan, M. *et al*. Self-assembled artificial cilia. *PNAS* **107**, 1844-1847 (2010).
12. Evans, B.A. *et al*. Magnetically actuated nanorod arrays as biomimetic cilia. *Nano Letters* **7**, 1428-1434 (2007).
13. den Toonder, J. *et al*. Artificial cilia for active microfluidic mixing. *Lab on a Chip* **8**, 533-541 (2008).
14. van Oosten, C.L., Bastiaansen, C.W.M. & Broer, D.J. Printed artificial cilia from liquid-crystal network actuators modularly driven by light. *Nature Materials* **8**, 677-682 (2009).
15. Stroock, A.D. *et al*. Chaotic mixer for microchannels. *Science* **295**, 647-651 (2002).
16. Yang, J.T., Tung, K.Y. & Li, C.C. Mixing and hydrodynamic analysis of a droplet in a planar serpentine micromixer. *Microfluidics and Nanofluidics* **7**, 545-557

(2009).
17. Ugaz, V.M. & Sudarsan, A.P. Fluid mixing in planar spiral microchannels. *Lab on a Chip* **6**, 74-82 (2006).
18. Hulsen, M.A., Kang, T.G., den Toonder, J.M.J., Anderson, P.D. & Meijer, H.E.H. A direct simulation method for flows with suspended paramagnetic particles. *Journal of Computational Physics* **227**, 4441-4458 (2008).
19. Hayes, M.A., Polson, N.A. & Garcia, A.A. Active control of dynamic supraparticle structures in microchannels. *Langmuir* **17**, 2866-2871 (2001).
20. Purcell, E.M. Life at Low Reynolds-Number. *American Journal of Physics* **45**, 3-11 (1977).
21. Richards, J.R., Beris, A.N. & Lenhoff, A.M. Steady laminar flow of liquid-liquid jets at high Reynolds numbers. *Physics of Fluids A* **5**, 1703-1717 (1993).
22. Meng, H. & Hussain, F. Holographic Particle Velocimetry - a 3d Measurement Technique for Vortex Interactions, Coherent Structures and Turbulence. *Fluid Dynamics Research* **8**, 33-52 (1991).
23. Elsinga, G.E., Scarano, F., Wieneke, B. & van Oudheusden, B.W. Tomographic particle image velocimetry. *Experiments in Fluids* **41**, 933-947 (2006).
24. Patrick, M.J., Chen, C.Y., Frakes, D., Dur, O. & Pekkan, K. Cellular-level near-wall unsteadiness of high-hematocrit erythrocyte flow using confocal μPIV. *Experiments in Fluids* **50**, 887-904 (2011).
25. Adrian, R.J. Twenty years of particle image velocimetry. *Experiments in Fluids* **39**, 159-169 (2005).
26. Chen, C.-Y., Menon, P., Kowalski, W. & Pekkan, K. Time-resolved OCT-μPIV: A new microscopic PIV technique for noninvasive depth-resolved pulsatile flow profile acquisition. *Experiments in Fluids* **54**, 1426 (2013).
27. Lindken, R., Westerweel, J. & Wieneke, B. Stereoscopic micro particle image velocimetry. *Experiments in Fluids* **41**, 161-171 (2006).
28. Calhoun, R. *et al*. Paramagnetic particles and mixing in micro-scale flows. *Lab on a Chip* **6**, 247-257 (2006).
29. Floyd, S., Diller, E., Pawashe, C. & Sitti, M. Control methodologies for a heterogeneous group of untethered magnetic micro-robots. *International Journal of Robotics Research* **30**, 1553-1565 (2011).
30. Wieneke, B. Stereo-PIV using self-calibration on particle images. *Experiments in Fluids* **39**, 267-280 (2005).
31. Calluaud, D. & David, L. Stereoscopic particle image velocimetry measurements of the flow around a surface-mounted block. *Experiments in Fluids* **36**, 53-61 (2004).